remote sensing

MDPI

Article

A Satellite-Based Climatology of Wind-Induced Surface Temperature Anomalies for the Antarctic

Günther Heinemann *, Lukas Glaw and Sascha Willmes

Environmental Meteorology, University of Trier, 54286 Trier, Germany

* Correspondence: heinemann@uni-trier.de; Tel.: +49-651-201-4623

Received: 15 May 2019; Accepted: 26 June 2019; Published: 28 June 2019

Abstract: It is well-known that katabatic winds can be detected as warm signatures in the surface temperature over the slopes of the Antarctic ice sheets. For appropriate synoptic forcing and/or topographic channeling, katabatic surges occur, which result in warm signatures also over adjacent ice shelves. Moderate Resolution Imaging Spectroradiometer (MODIS) ice surface temperature (IST) data are used to detect warm signatures over the Antarctic for the winter periods 2002–2017. In addition, high-resolution (5 km) regional climate model data is used for the years of 2002 to 2016. We present a case study and a climatology of wind-induced IST anomalies for the Ross Ice Shelf and the eastern Weddell Sea. The IST anomaly distributions show maxima around 10–15K for the slopes, but values of more than 25K are also found. Katabatic surges represent a strong climatological signal with a mean warm anomaly of more than 5K on more than 120 days per winter for the Byrd Glacier and the Nimrod Glacier on the Ross Ice Shelf. The mean anomaly for the Brunt Ice Shelf is weaker, and exceeds 5K on about 70 days per winter. Model simulations of the IST are compared to the MODIS IST, and show a very good agreement. The model data show that the near-surface stability is a better measure for the response to the wind than the IST itself.

Keywords: katabatic winds; MODIS ice surface temperatures; ice shelves; Antarctic

1. Introduction

The near-surface wind field over the Antarctic ice sheet (Figure 1a) is dominated by katabatic winds in the stably-stratified boundary layer [1–3], which is a climatological feature for the Antarctic continent [4]. Katabatic winds may rise up to gale force [5,6], and are important for the exchange of energy and momentum between the atmosphere and the underlying surface, but also for field work. While the classical katabatic (downslope) winds develop only over the slopes of the ice sheet, they can extend also over adjacent (flat) ice shelves, if appropriate synoptic forcing and/or topographic channeling is present. These are the so-called katabatic surges. Despite the fact that the katabatic wind is a negatively buoyant air layer, the strong wind associated with katabatic winds and surges leads to a warm signature of the surface temperature. The reason for this behavior is the strong turbulence in katabatic winds [7], which destroys or weakens the surface inversion compared to the weak-wind surroundings, where the surface inversion leads to much colder temperatures (Figure 2). This leads to a warming close to the surface, while the katabatic wind layer as a whole is still negatively buoyant. Thus the regions of strong wind over ice sheets and ice shelves can be detected as warm signatures in satellite thermal infrared (TIR) imagery, particularly in winter, when the surface inversions are at their strongest (see [8]).

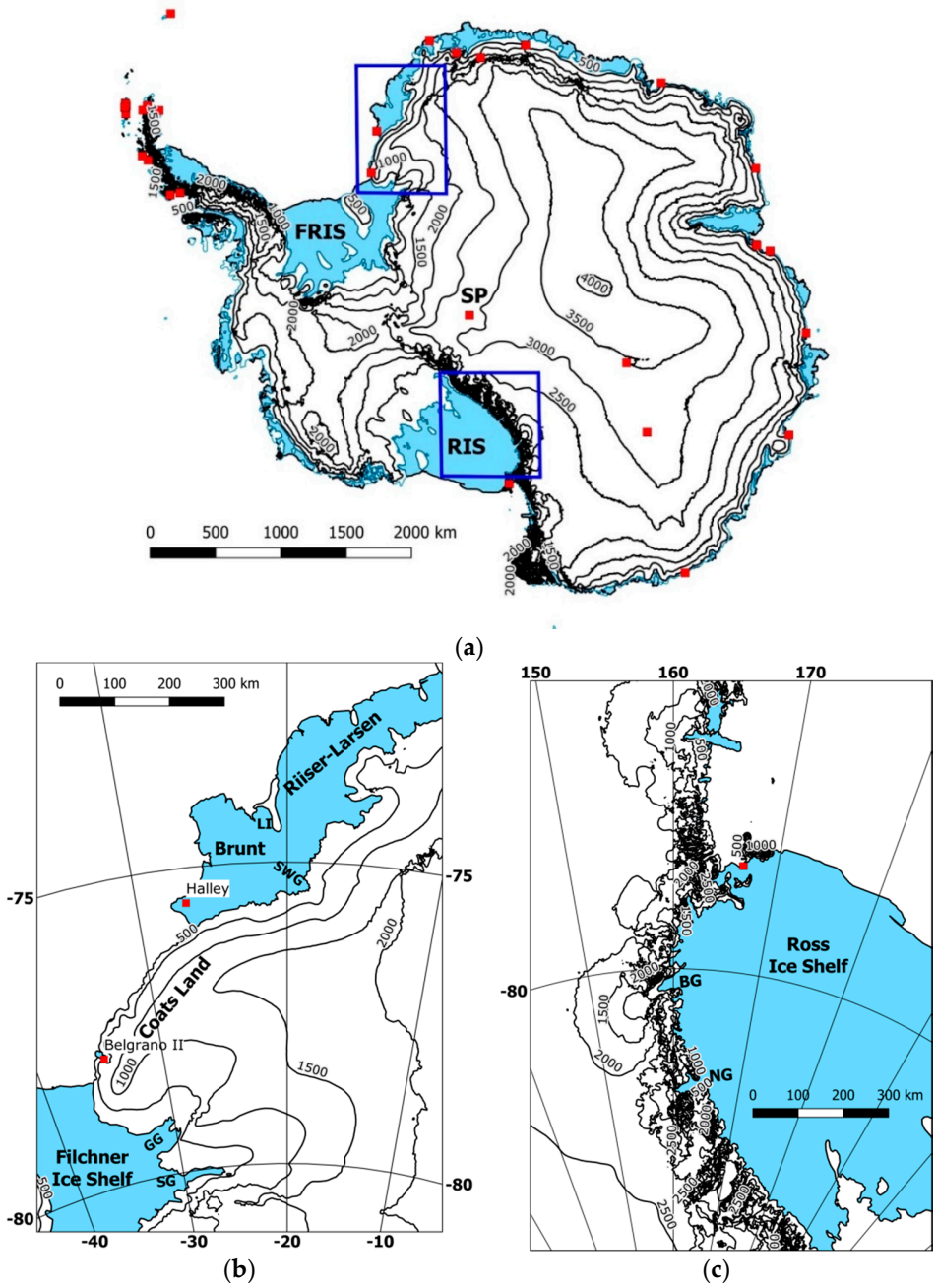

Figure 1. (**a**) Map of the Antarctic with topography (isolines). Permanent research stations are marked by red squares. Ice shelf areas are light blue (FRIS = Filchner-Ronne Ice Shelf, RIS = Ross Ice Shelf). The blue rectangles mark the focus areas of this study. Data source: RAMP2 ([9]). Part (**b**): As (**a**), but for the study area in the eastern Weddell Sea with SWG = Stancomb-Wills Glacier, LI = Lyddan Island, GG = Goldsmith Glacier, SG = Slessor Glacier. Part (**c**): As (**a**), but for the study area of the Ross Ice Shelf with BG = Byrd Glacier, NG = Nimrod Glacier.

These warm signatures in TIR data were first explained by [10] and further investigated by [11–14]. They can also be found in high-resolution numerical model simulations [15]. An example of katabatic warm signatures including a katabatic surge on 2 August 2015 is shown in Figure 3 for the area of the eastern Weddell Sea (compare Figure 1b). The katabatic surge extends from the Stancomb-Wills Glacier over the Brunt Ice Shelf. Warm katabatic signatures are present over the slopes of Coats Land and in the valley associated with the Goldsmith Glacier. Under favorable synoptic conditions, katabatic surges can travel over long distances over the flat ice shelves and can lead to the formation of coastal polynyas [16].

Katabatic flows are also considered to contribute to the formation of mesocyclones in the coastal regions [1,12,17]. For example, [18] relate the formation of a mesocyclone near Halley to a katabatic surge at Stancomb-Wills Glacier.

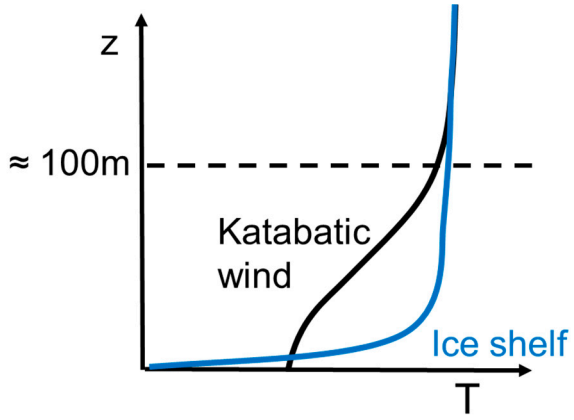

Figure 2. Schematics of the vertical temperature structure in the katabatic wind (black line) and a weak-wind ice surface (blue line).

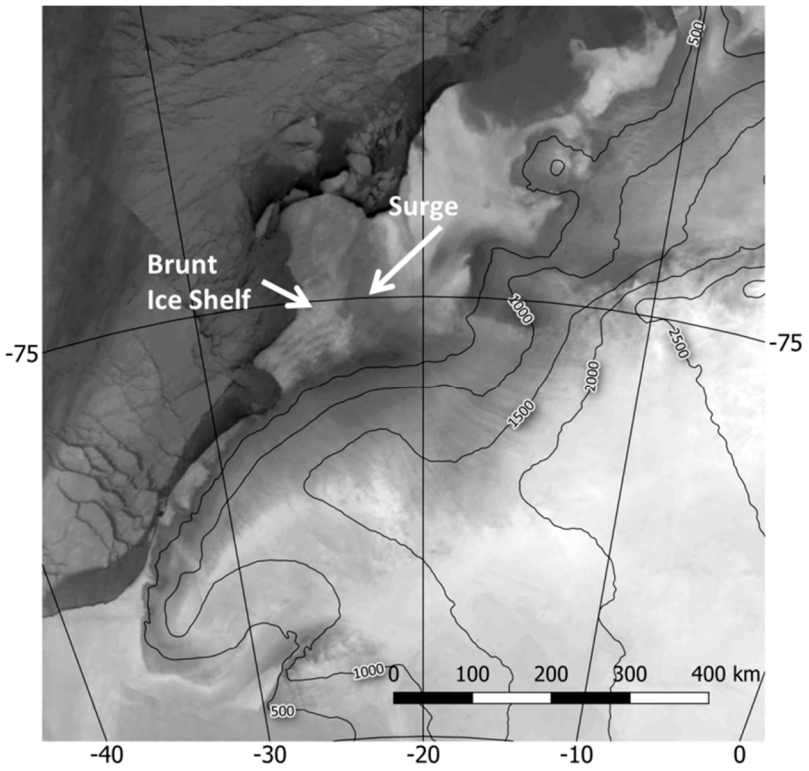

Figure 3. Example of katabatic warm signatures (Moderate Resolution Imaging Spectroradiometer (MODIS) IR image 2 August 2015, warm = dark, data source: NASA Worldview) and topography from Cryosat-2 data [19]).

In the present study, Moderate Resolution Imaging Spectroradiometer (MODIS) ice surface temperature (IST) data are used for the detection of warm signatures over the Antarctic ice sheet and the ice shelves. MODIS data are available since 2002 and have been used for studies of the surface temperature in the Antarctic by e.g., [20–22]. [23] used MODIS IST for the assessment of atmospheric reanalyses. Here we present an analysis of wind-induced warming for the winter periods 2002–2017.

The focus lies on a climatology of wind-induced IST anomalies for the Ross Ice Shelf (Figure 1c) and the eastern Weddell Sea (Figure 1b).

2. Materials and Methods

2.1. MODIS Surface Temperature Products

We use the Moderate Resolution Imaging Spectroradiometer (MODIS) land surface temperature product MOD11 (Terra satellite) and MYD11 (Aqua satellite), in the following referred to as MxD11 [24], and the ice surface temperature product MOD/MYD29 (Terra/Aqua), in the following referred to as MxD29 [25]. Both products are used as collection 6 Level-2 swath data, and have a spatial resolution of 1 km at nadir. All swaths for the austral winter seasons (April to September) from 2002 to 2017 were used south of 50°S, resulting in ca. 160 swaths per day.

In a first step, the data of the surface temperature from MxD11 and MxD29 were merged in order to cover ice sheet and ice shelf regions seamlessly using the same swaths from each product. Ice surface temperature (IST) data from each swath were then projected to a polar stereographic grid with a pixel resolution of 1.5 km for the whole of the Antarctic. A daily average was computed for each pixel using the median of all available IST values in the daily stack. Figure 4 shows the mean daily coverage of cloud-free pixels for the whole Antarctic. The highest frequency of cloud-free pixels can be seen over the ice sheet for surface elevations higher than 2000 m. Since synoptic weather systems are often blocked by the high topography, frontal systems associated with clouds are rare over the Antarctic plateau region [26]. Although the MxD11 and MxD29 data were merged seamlessly, a difference in the cloud detection of these products becomes apparent. MxD11 seems to reject more pixels because of cloudiness, leading to a jump in the frequency of cloud-free pixels between ice shelves and the continental slopes. However, the mean coverage in the latter regions is at least between 2–4 per day, i.e., there is a good spatial coverage for monthly means. In order to minimize errors caused by the cloud detection in the different data sets, a minimum requirement of at least three observations per pixel per day was used.

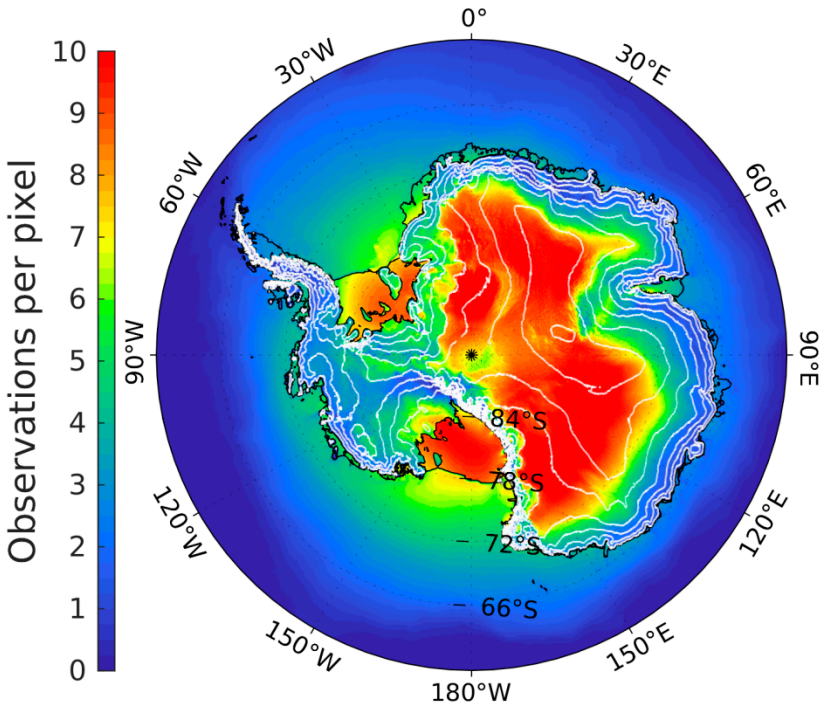

Figure 4. Mean daily coverage 2002–2017 of cloud-free pixels (topography as isolines every 500 m).

Monthly means of the IST were calculated from the daily averages. In order to quantify the katabatic warm signatures, an anomaly was computed as the temperature difference between a region affected by the katabatic wind and a reference region, where no or only weak warming effects due to katabatic winds or surges are present.

The daily anomaly for each pixel was calculated based on the difference between the daily value and the monthly mean surface temperature in the reference region and then averaged as monthly, seasonal or overall means (for details see Section 3).

2.2. Model Data

The non-hydrostatic regional climate model COSMO-CLM (CCLM, [27]) was used to produce a high-resolution atmospheric data set for the years 2002 to 2016. The model is nested in ERA-Interim data [28] and uses high-resolution sea-ice concentration data [29] on a daily basis to keep the hindcast close to reality. The model was adapted to the polar regions by the implementation of a thermodynamic sea-ice model [30–32]. The model was run for the Weddell Sea region with resolutions of 15 and 5 km using a similar set-up as in [15]. Data is available every hour. Data of the model with 5 km resolution are used in this study.

3. Results

3.1. Overview

Figure 5 shows the mean cloud-free surface temperature for all winters. For this composite, a total of about 460,000 swaths have been processed. A lot of details can be seen, e.g., the cold signal of iceberg A23A in the Weddell Sea north of Berkner Island, warm signals in regions of reoccurring coastal polynyas (such as in Terra Nova Bay) and warm katabatic signals (warm thermal belt [13]) almost in all coastal regions. In the following, we will focus on the regions of the Ross Ice Shelf (Figure 1c) and the eastern Weddell Sea (Figure 1b).

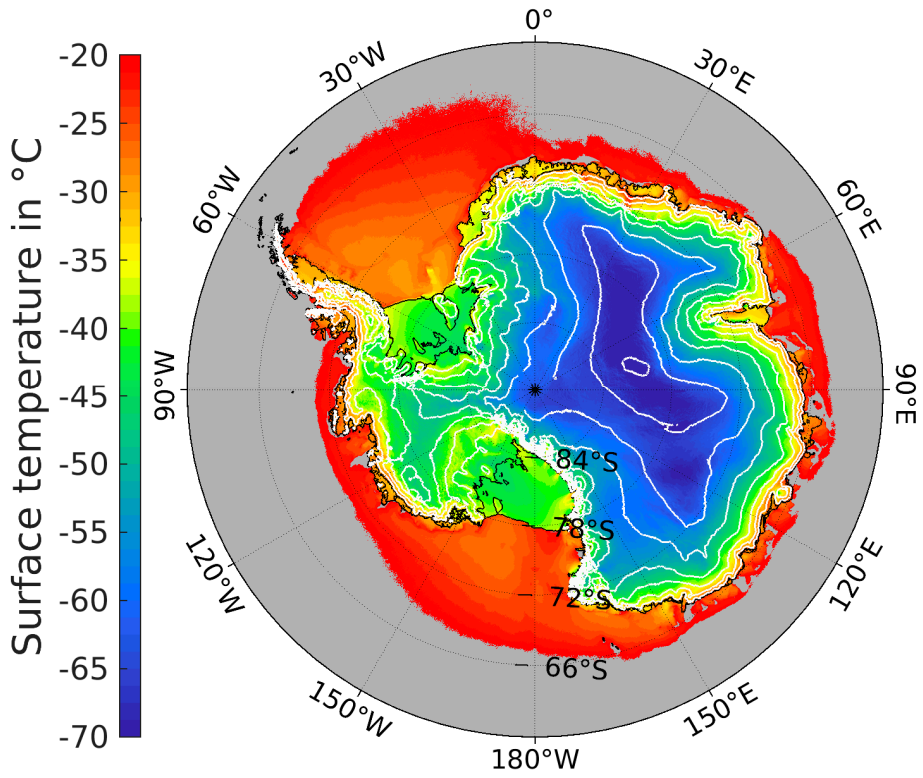

Figure 5. Mean cloud-free surface temperature for winter (April–September) 2002 to 2017 (isolines = topography every 500 m, temperatures outside the range in grey).

3.2. Ross Ice shelf (RIS)

The mean surface temperature anomaly for the RIS for all winters is shown in Figure 6. The method for computing the anomalies is described in Section 2, and the reference area is marked in Figure 6.

The positions of strong warm anomalies agree with the outlets of the main glaciers, particularly with the Byrd Glacier and the Nimrod Glacier (see Figure 1c). The katabatic warm signal associated with the outflow of these regions extends more than 100 km over the ice shelf, and for the Byrd Glacier it even extends to the front of the RIS. This may also reflect the fact that under suitable synoptic conditions, katabatic surges are found as flows parallel to the Transantarctic Mountains, which are fed also by the katabatic outflow of both the Byrd Glacier and Nimrod Glacier [12].

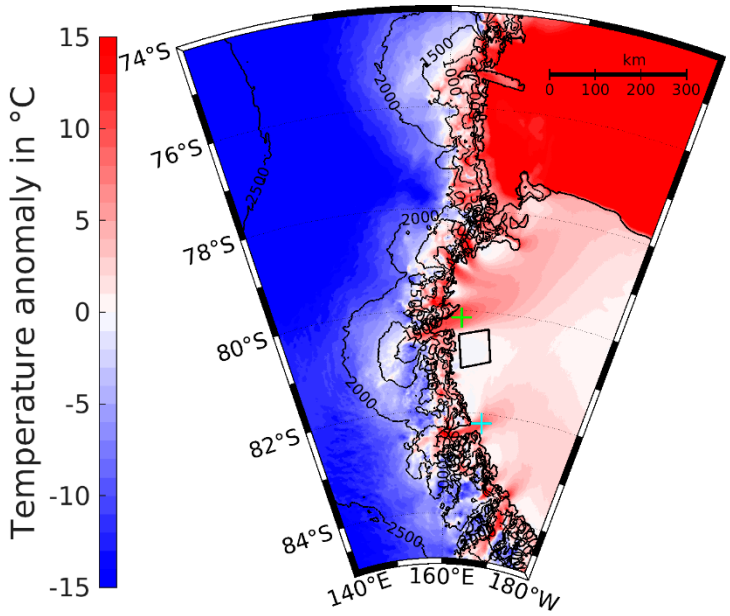

Figure 6. Mean surface temperature anomaly for the RIS for winter (April–September) 2002 to 2017 (isolines = topography every 500 m). The reference area is marked by the box over the ice shelf, the exit areas for both the Byrd and Nimrod glaciers (see Figure 1c) are marked by crosses.

The surface temperature anomaly distribution for all winters for the exit regions of the Byrd Glacier and the Nimrod Glacier is presented in Figure 7. For the Byrd Glacier, the highest frequencies are found for anomalies between 8–15K, but 20K are also exceeded. For the Nimrod Glacier, the peak is at approximately the same values, but the distribution is broader and values of more than 25K are found as well. Anomalies exceeding 5K are found on 146 and 123 days per winter for Byrd and Nimrod Glacier, respectively. This corresponds to 80% of all days and 82% of observed days for the Byrd Glacier and 67% of all days and 72% of observed days for the Nimrod Glacier. The statistics for different months are shown in Figure 8. Median values for Byrd Glacier increase from around 8K in April/May to 10K in July, and stay relatively constant through August and September. The highest 10% of the anomalies exceed 18K in winter. The same behavior can be seen for Nimrod Glacier, but with anomalies being weaker by around 2K, and with a larger spread of values. The interannual variability of the anomalies is relatively small (see supplement Figure S1).

3.3. Eastern Weddell Sea

3.3.1. IST Climatology

The mean surface temperature anomaly for the Eastern Weddell Sea for all winters is shown in Figure 9. The reference area is in a region of the Brunt Ice Shelf (BIS) that is generally not affected by

katabatic surges, which mainly occur in the region of the Stancomb-Wills Glacier (SWG, see Figure 1b). A strong warm anomaly can be seen at the end of the slopes of Coats Land and the BIS. Unlike the signatures found for the RIS, katabatic surges (see Figure 3) are not detected as a signal in the mean anomaly. The reference area for the surge anomaly was chosen on the BIS close to the slope, being in the region of expected surges (see Figure 3). Besides the warm signals of katabatic winds over the slopes and katabatic surges of the ice shelves, a lot of small-scale structures can be seen over the ice sheet (Figure 9). While the small-scale warm anomaly at the Goldsmith Glacier in the western part of FIS (see Figure 1b) can be attributed to the convergence of the katabatic wind at the steep southern slope of this glacier valley, other features seem to be related to small structures in the surface elevation of the ice sheet (see supplement Figure S2).

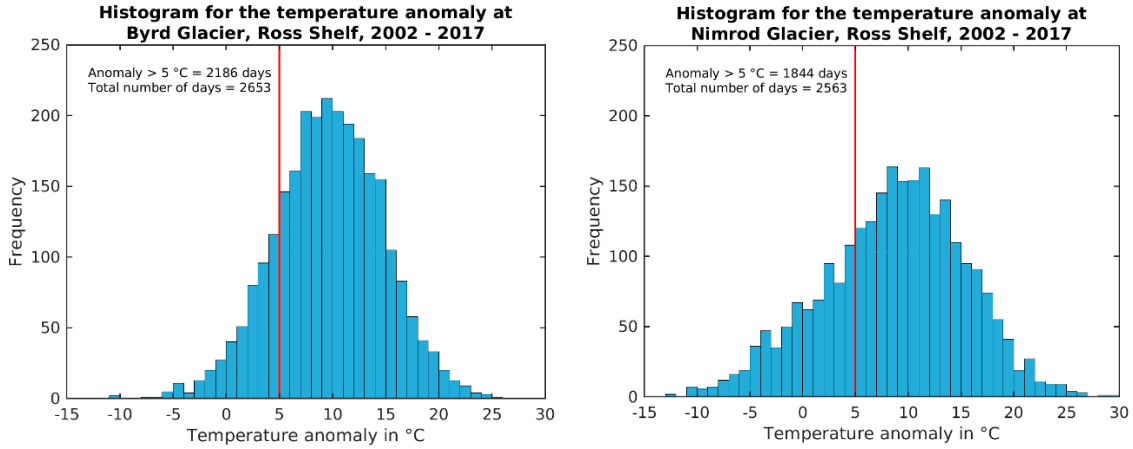

Figure 7. Surface temperature anomaly distribution (1K bins) for winter (April–September) 2002 to 2017 for the exit regions of a) Byrd Glacier and b) Nimrod Glacier (marked by crosses in Figure 6). The red line marks a value of +5°C.

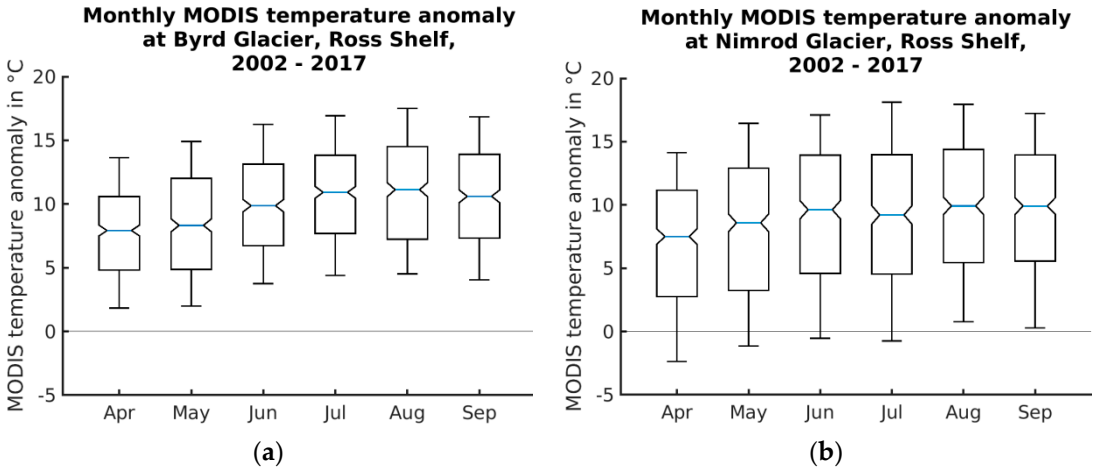

Figure 8. Box-whisker plot for the surface temperature anomaly for different months for winter (April–September) 2002 to 2017 for Byrd Glacier (**a**) and Nimrod Glacier (**b**). The median, the 25 and 75% percentiles are plotted as the box, the 10 and 90% percentiles are plotted as error bars.

The anomaly statistics for the slope area (Figure 10a) for all winters show the highest frequencies found between 8–15K, which is comparable to the RIS. In extreme cases values of more than 20K are found. Only few cases show negative values. For the surge region, a high amount of negative values is found. The positive peak is at lower values (6–7K), but values of more than 20K are found as

well. Anomalies exceeding 5K are found on 76 and 72 days per winter for the slope and surge area, respectively. This corresponds to 42% of all days and 80% of observed days for the slope area and 39% of all days and 43% of observed days for the surge area. The statistics for different months are shown in Figure 11. The highest anomalies for the slope area occur in September, but the differences between different months are relatively small. For the surge area, median values reach only 2–3K, and the 25% percentile is negative for all months. 10% of the anomalies exceed 11–13K, indicating that strong katabatic surges occur less frequently than for the RIS. As for the RIS, the interannual variability of the anomalies is relatively small, only for 2013 a median value close to zero is found for the surge area (see supplement Figure S3).

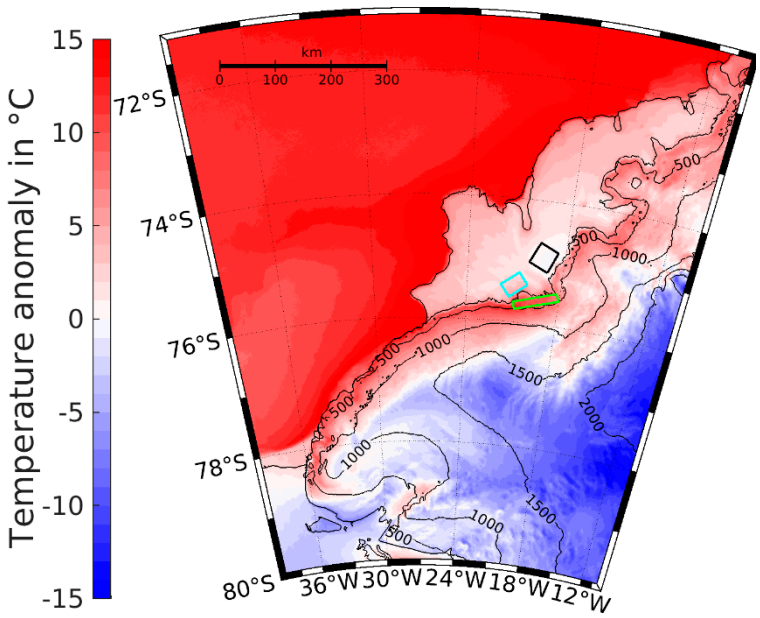

Figure 9. As Figure 6, but for the eastern Weddell Sea. The green box marks the slope area, the blue box marks the surge area, the black box marks the reference area.

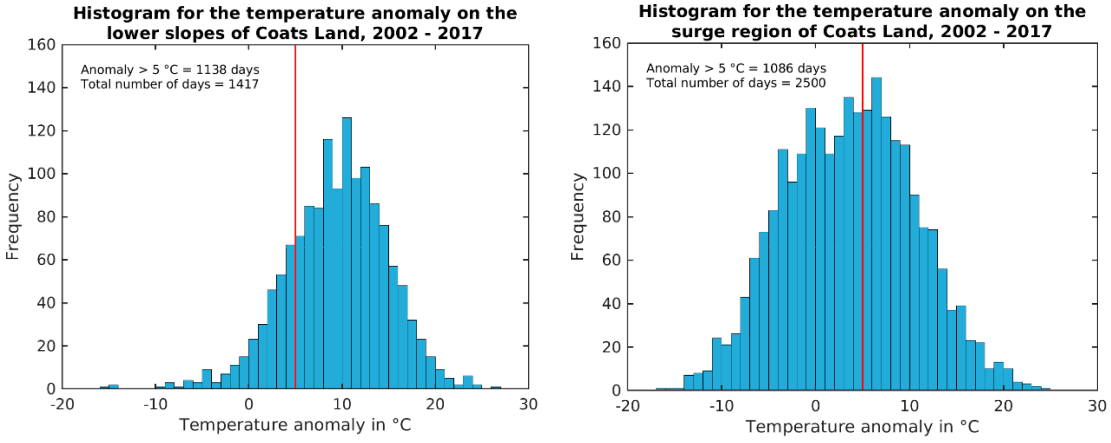

(**a**) (**b**)

Figure 10. As Figure 7, but for the eastern Weddell Sea for (**a**) the slope area and (**b**) the surge area.

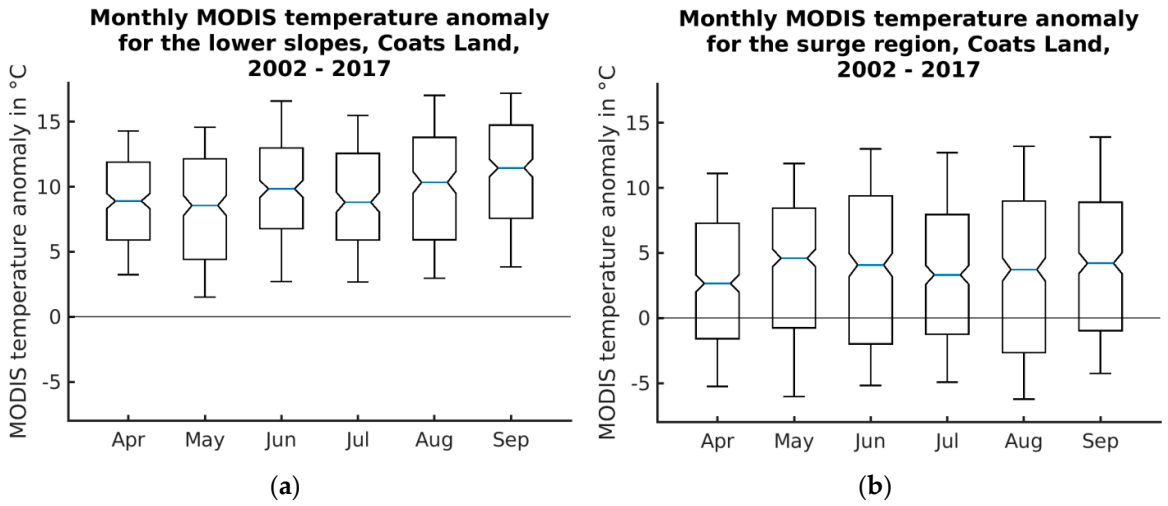

Figure 11. Box-whisker plot for the surface temperature anomaly for different months for winter (April–September) 2002 to 2017 for the eastern Weddell Sea for the slope (**a**) and surge areas (**b**). The median, the 25 and 75% percentiles are plotted as the box, the 10 and 90% percentiles are plotted as error bars.

3.3.2. IST Relation to CCLM-simulated Wind

In order to study the relation of the katabatic warming signal to the wind, we first compare the MODIS IST to CCLM-simulated wind and IST fields for a case study. Figure 12 shows the daily series of these fields for 30 April–2 May 2014. This case study demonstrates a katabatic wind situation with a duration of five days (29 April–3 May 2014). On 30 April, a pronounced warm belt structure can be seen in the MODIS IST over the slopes of Coats Land extending from the Filchner Ice Shelf to the Stancomb-Wills Glacier. Temperatures over the Brunt Ice Shelf (BIS) and Riiser-Larsen Ice Shelf (RLIS) are significantly colder (temperatures 10–20K lower). The higher IST values over the BIS indicate the starting katabatic surge, which is well developed on the next two days. On 1 May, the warm temperatures associated with the katabatic surge reach the edge of the BIS. On 2 May, the katabatic surge shifts to the north and travels over a distance of about 250 km across the BIS. The daily data of the CCLM model with 5 km resolution can reproduce the observed temperature patterns (Figure 12, right column). The warm belt structure over the slopes is associated with strong katabatic winds. The katabatic surge develops with the increasing influence of a synoptic cyclone over the eastern Weddell Sea. The synoptic support leads to the extent of the katabatic flow over the BIS being almost in geostrophic balance. On 3 May, a cyclone over the central Weddell Sea approaches the region from the west. This leads to a northeasterly wind along the Luitpold Coast and ends the katabatic surge.

The good agreement between IST from MODIS and CCLM allows one to study the relation of katabatic warm signals and the wind speed. Figure 13 shows the daily IST values for the slope and surge areas as well as the CCLM wind speed for April and May 2014. The high peaks in the IST and wind speed values (up to 20 ms^{-1}) at the end of April correspond to the case study discussed in Figure 12. A similar signal is present on 16 April. The IST changes are the largest for the surge region over the ice shelf. It is also obvious that there are more data gaps over the slope, which results also from the fact that two different data sets are used (see Section 2.1).

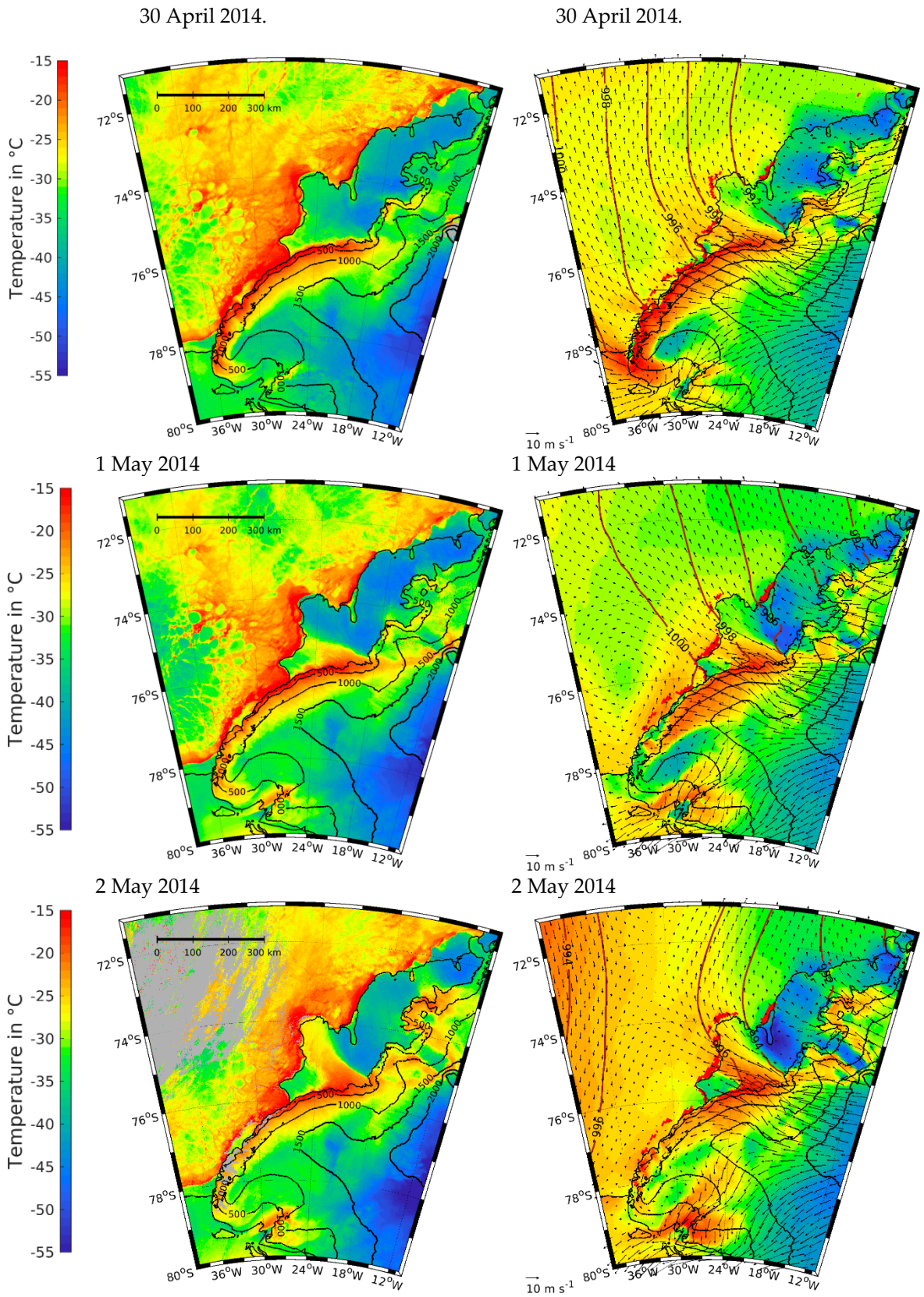

Figure 12. Daily composite of MODIS surface temperature (left column) and simulated CCLM daily averages of surface temperature, MSLP (isolines) and 10m-wind vectors (right column) for 30 April 2014 (upper row), 1 May 2014 (middle row) and 2 May 2014 (lower row).

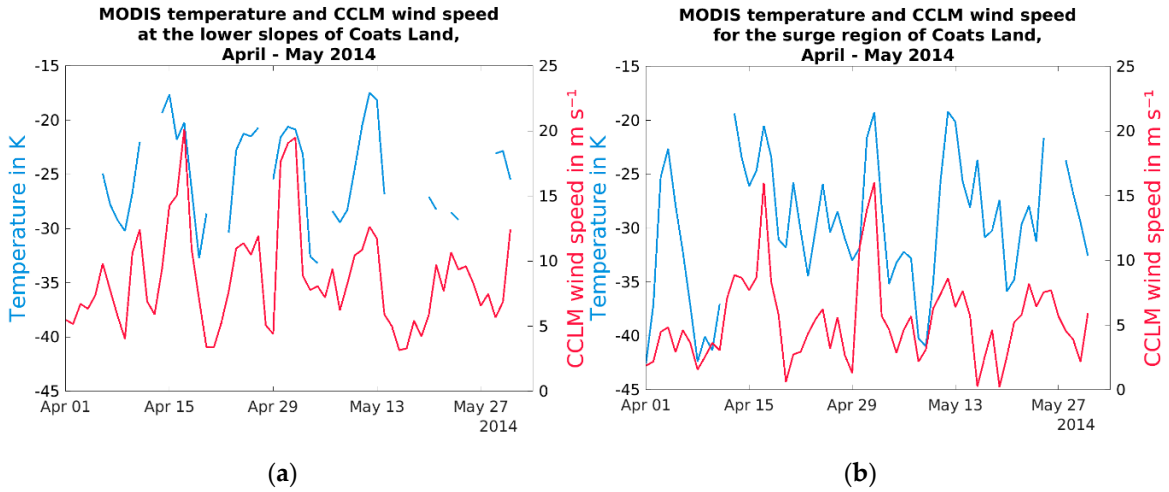

Figure 13. Time series of daily averages of MODIS ice surface temperature (IST) (blue) and CCLM 10 m-wind speed (red) for the slope (**a**) and surge areas (**b**) for April and May 2014.

A comparison of simulated IST from CCLM with the MODIS IST (both as daily values) is shown in Figure 14 for the surge region. For April and May 2014, a very good correlation (r^2 of 66%) is found for the two data sets using a linear regression (Table 1). In the average, CCLM IST are too warm by 3–5K. This warm bias is also present for all winters 2002–2016, while the correlation is only slightly lower. For the slope and reference areas, the correlation is slightly larger (r^2 of 71% and 67%, respectively) for all winters 2002–2016 (see supplement Figure S4 and Table S1).

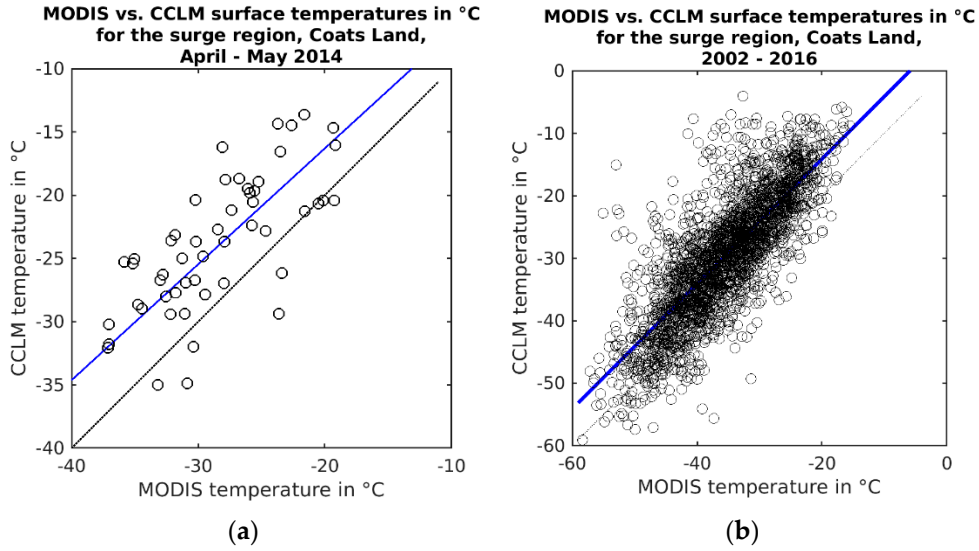

Figure 14. IST from MODIS and CCLM for the surge area for April and May 2014 (**a**) and for winters 2002–2016 (**b**). The blue line indicates the linear fit.

The relation between CCLM wind and IST for the surge area is shown in Figure 15. Since the IST of the reference area is also sensitive to wind, the differences between the surge area and reference area were chosen for daily values (only days with positive differences are accounted for). For April and May 2014, a significant linear relation is found ($p < 0.01$, $r^2 = 0.72$, Table 1).

When using only data with wind directions corresponding to a downslope wind (directions 90–180°), the coefficient of determination is even improved ($r^2 = 0.83$). For all of the winters of 2002–2016, still a reasonable r^2 is found ($r^2 = 0.44$ and $r^2 = 0.35$ for the downslope and all directions, respectively, Figure 15b). For the slope region, the correlation is reasonable for April and May 2014

(r^2 = 0.41), but the explained variance is only 0.25 to 0.29 for the whole period (see supplement Figure S5 and Table S1).

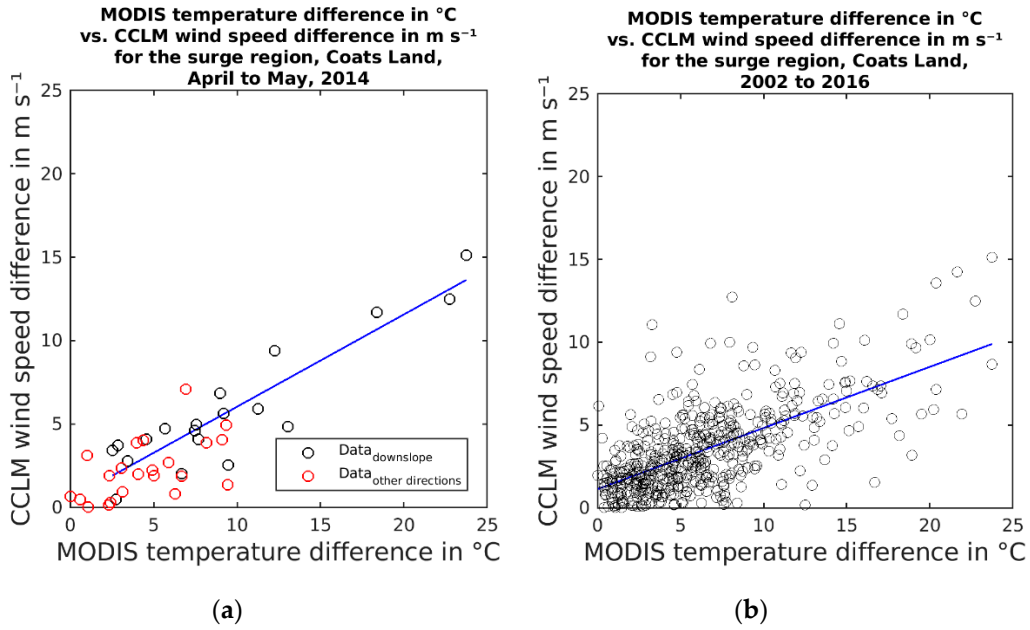

Figure 15. IST difference between surge area and reference area and corresponding CCLM 10 m-wind speed difference for (**a**) April and May 2014 for all days (red symbols) and days with the downslope wind (black symbols) and (**b**) winters 2002–2016 for the days with the downslope wind. The blue line indicates the linear fit.

The period of April and May 2014 is an exceptionally long period with almost no clouds in the eastern Weddell Sea, which reduces potential errors in the daily IST product. But other factors, such as the presence of drifting snow, could potentially decrease the correlation between wind and IST [33,34]. However, the largest influence on the relation between IST and wind is given by the processes in the atmospheric boundary layer. It is also obvious from Figure 13 that the IST response to the wind is not linear, since a large temperature change can be associated with a large change in wind speed (30 April 2014), but also with a relatively small change in wind speed (12 May 2014). These ambiguities are confirmed by the results of the simulations for the relation between wind and IST, selecting the same days as for the MODIS comparison for 2002–2016 (see supplement Figure S6, Figure S7 and Table S1). For the surge area, the model-based correlation is slightly higher than for the MODIS results (r^2 = 0.51), and for the slope area the correlation is comparable to the MODIS results (r^2 = 0.38 for downslope winds).

Table 1. Statistics for the linear regressions (y = a + bx) of the different Figures (n = number of values, a = interception, b = slope, with dimensions). Wind is always from CCLM. All regressions are significant with a p value less than 0.01.

Figure	x	y	r	r^2	RMSE	n	b		a	
14a	IST MODIS	IST CCLM	0.81	0.66	4.06	58	0.92		2.01	°C
14b	IST MODIS	IST CCLM	0.80	0.64	5.92	2347	1.00		5.85	°C
15a (all data)	IST diff. MODIS	wind diff.	0.85	0.72	1.79	42	0.52	m/(sK)	0.23	m/s
15a (downslope)	IST diff. MODIS	wind diff.	0.91	0.83	1.61	19	0.55	m/(sK)	0.51	m/s
15b (all data)	IST diff. MODIS	wind diff.	0.59	0.35	1.54	1516	0.32	m/(sK)	1.32	m/s
15b (downslope)	IST diff. MODIS	wind diff.	0.66	0.44	1.88	517	0.37	m/(sK)	1.13	m/s
16a	T2m-IST CCLM	wind	0.82	0.68	0.97	1925	-0.44	m/(sK)	7.34	m/s
16b	T2m-IST CCLM	wind	0.77	0.59	1.56	764	-0.72	m/(sK)	9.05	m/s

The IST is a result of the energy balance terms at the snow surface and their interactions with the lower boundary layer. For example, the IST (as well as the near-surface temperature) reacts on changes of the incoming longwave radiation on a short time scale [35]. The sensible heat flux is a function of the near-surface stability and the wind speed. The atmospheric boundary layer over polar ice surfaces is generally stably stratified for cloud-free conditions, and an increase in wind speed leads to a higher sensible heat flux towards the surface and a decrease of the near-surface stability due to enhanced generation of turbulence by wind shear [7]. The CCLM simulations can be used to further explore the process of the change of the surface inversion due to the wind. Figure 16 shows the difference between the temperature at 2 m (T2m) and the IST for all CCLM grid points over ice shelves and over the lower slope area (50–500 m) for the eastern Weddell Sea for 2 May 2014 (cf. Figure 12). There is a clear relation between the near-surface stability (T2m-IST) and the wind speed for wind speeds lower than 6 m/s, but for high wind speeds the scatter is large. For T2m-IST values exceeding 3K a high correlation between near-surface stability and wind speed is found for the ice shelf and for the slope (r^2 = 0.68 and r^2 = 0.59, respectively). The near-surface stability is a better measure for the sensitivity to the wind than the IST itself, since it is less sensitive to the spatial gradients in temperature (see supplement Figure S8). However, only IST is measurable by MODIS, which underlines the value of high-resolution simulations of the Antarctic boundary layer in understanding the wind-induced warming.

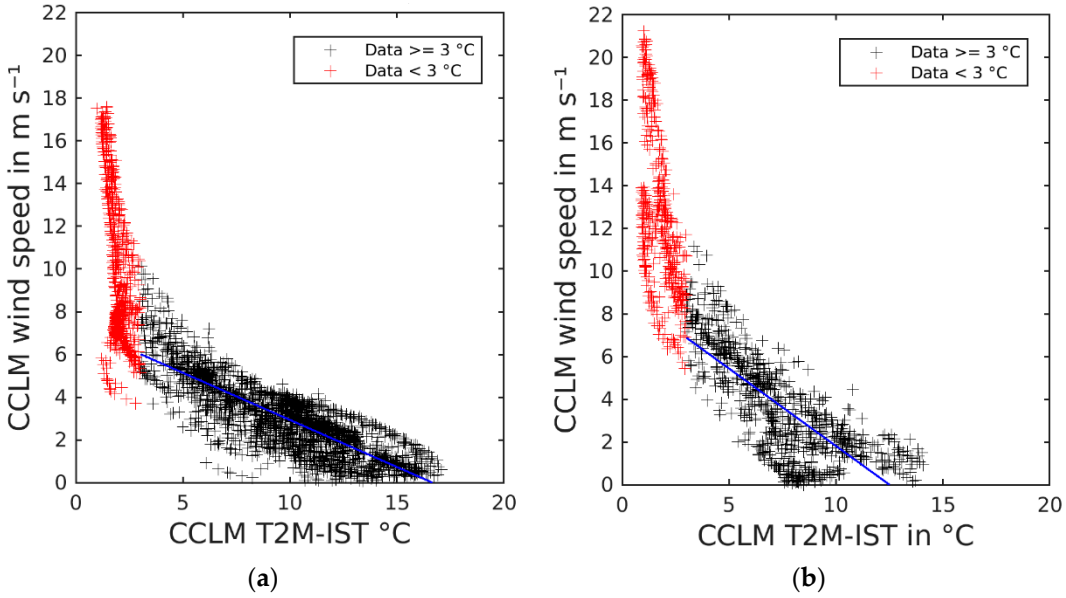

Figure 16. CCLM (T2m-IST) difference as a function of wind speed as for the daily means for 2 May 2014 (**a**) for the ice shelf areas of BIS and Riiser-Larsen (RLIS) and (**b**) for the slope area for the height range 50–500 m (temperatures height-corrected with an adiabatic lapse rate). The blue line indicates the linear fit for (T2m-IST) > 3K.

4. Discussion

Warm signatures in the surface temperature related to katabatic winds and katabatic surges in the Antarctic have been reported in a number of studies previously. [13] show that the surface temperature field derived from Advanced Very High Resolution Radiometer (AVHRR) infrared imagery for the years 1993 and 1995 (a total of 53 images) typically show a warm thermal belt over the slopes of Coats Land in the Weddell Sea. This implies that the katabatic flow does not reach the Brunt Ice Shelf (BIS), where the surface is colder, and a strong surface inversion is present. The temperature difference between the slope and BIS is at its largest in the winter (March-August) with values of 11–15K. Our results agree with this study, as the warm belt is clearly seen in Figure 9. The distribution of temperature anomalies (Figure 10a) cover a much broader range than shown in [13], because the

present study is based on data for 15 years, and includes more than 1400 days. The IST anomaly distributions show maxima around 10–15K for the slopes, but values of more than 25K are also found.

For the RIS, the classical study of [10] evaluates warm IST signals associated with katabatic surges using daily Defense Meteorological Satellite Program (DMSP) infrared imagery for the winters 1984 and 1985 (April–October). Clear-sky images covering the north-western RIS were obtained on 32% of the days. The exit of Byrd Glacier was found to be the most prominent feature of warm signatures (87% occurrence frequency), while Nimrod Glacier had only a 3% occurrence frequency of warm signatures. In our long-term study, we find only small differences in warm anomalies for these two glacier regions. Anomalies exceeding 5K are found on 82% of observed days for the Byrd Glacier and for 72% of observed days for the Nimrod Glacier.

The reason for the warm katabatic signatures is that the strong turbulence in katabatic winds [7] weakens the surface inversion compared to the weak-wind surroundings over the ice shelves (see Figure 2). In accordance with previous studies, e.g., [10,11,13,16], it was therefore the working hypothesis of the present paper that warm signatures are related to the wind speed or wind speed difference between areas influenced by katabatic flows (slope and surge areas) and undisturbed areas of the ice shelves. This relation between wind and IST anomalies could be demonstrated for case studies (Figure 12), but for the climatology of 15 winters, the relation between wind (from a high-resolution (5 km) regional climate model) and IST (from MODIS) is less well defined (correlation of 0.66 for the surge region and 0.54 for the slope).

Since the comparison of IST from MODIS and IST from the simulations showed a very good agreement, the relation of wind and IST was further examined using only model data. Using the model-based near-surface stability (difference between temperature at 2 m and the surface), a high correlation between near-surface stability and wind speed is found for the ice shelf and for the slope for wind speeds less than about 6 m/s. For higher wind speeds (or T2m-IST values smaller than 3K) the scatter is large. Thus there is a strong non-linear behavior of the response of the near-surface stability to the wind. For the high wind speeds which are generally associated with the katabatic winds over the slopes, wind speed changes have almost no effect on the near-surface stability. A similar behavior was found by [8] investigating inversions over the Antarctic plateau for the period 1994–2003. For the strongest inversions (90% percentile), a linear decrease in inversion strength is found with increasing wind for wind speeds up to 8 m/s.

In summary, the near-surface stability is found to be a better measure for the response to the wind than the IST itself, since it is less sensitive to the spatial gradients in temperature. The change of the boundary layer temperature structure is the primary signal of the wind response, but it has also feedbacks on the wind, the surface energy balance and the structure of the surface. Katabatic winds are a result of a stable boundary layer over sloped terrain, and the inversion strength influences strongly the wind intensity [36]. On the other hand the turbulent mixing reduces the inversion strength. Inversion strength and inversion height over the Antarctic slopes are much weaker/lower compared to the Antarctic plateau [37,38].

IST signatures in the form of streaks have been considered as an indicator of katabatic flows by [11,14]. For Greenland, these katabatic streaks are linked to topographic structures [14]. For the present study, streaks are not found in the long-term mean for the Antarctic. Streaks are present for individual katabatic wind cases (see Figure 3), but they are smoothed out evenly by the daily composites (see Figure 12). However, small-scale IST anomaly structures are present in the climatology that are related to the channeling of the katabatic wind in valleys, but also by structures in the surface elevation of the ice sheet (see supplement Figure S2).

Wind-induced warming is relevant for the surface energy balance, the snow structure and the surface melting over the Antarctic ice shelves. For the winter period studied in this paper, melting is very unlikely for the areas investigated. But similar warming effects are also present in the summer season, and the relation to melting is part of the study of [39]. They show that katabatic winds during summer lead to a wind-induced warming of >3K and a doubling of the surface melt in the grounding

zone. In addition, these winds cause areas with lower surface albedo (e.g., blue ice), which enhances melting. This preconditioning of the surface takes place also during winter, since the relatively warm (and dry) katabatic surges are associated with high latent heat fluxes. The blue ice areas at the exit region of the Stancomb-Wills Glacier on the BIS (see Figure 1b and Figure S2 in the supplement) indicate these effects of the katabatic surges.

The present study has the focus on the Ross Sea and Weddell Sea areas of the Antarctic. Future research directions will be the expansion of these studies to other areas using a combination of satellite and model data.

5. Conclusions

MODIS ice surface temperature (IST) data are used for the detection of warm signatures over the Antarctic for the winter periods 2002–2017. In addition, high-resolution (5 km) regional climate model data is used for 2002 to 2016.

For the first time, we present a climatology of wind-induced IST anomalies for the Ross Ice Shelf and the eastern Weddell Sea. The IST anomaly distributions show maxima around 10–15K for the slopes, but values of more than 25K are also found. Katabatic surges represent a strong climatological warming signal, which has impacts on the surface energy balance and the surface characteristics (such as the melting and the formation of blue ice areas).

The IST response to the wind is not linear, and is a result of all energy balance terms of the snow surface and their interaction with the lower boundary layer. While MODIS yields only the IST, the synergy with atmospheric model data allows for a deeper analysis. Using the model-based near-surface stability, a high correlation between near-surface stability and wind speed is found for the ice shelf and for the slope for wind speeds less than about 6 m/s.

Supplementary Materials: The following are available online at http://www.mdpi.com/2072-4292/11/13/1539/s1. Figure S1: Box-whisker plot for the IST anomaly for different years for winters 2002 to 2017 for Byrd Glacier (a) and Nimrod Glacier (b). Figure S2: Subarea of Figure 9 for a) the IST anomaly for winter seasons 2002 – 2017 and b) the Cryosat-2 topography and hillshade. Figure S3: as Figure S1, but for the eastern Weddell Sea for the slope (a) and surge areas (b). Figure S4: IST from MODIS and CCLM for the (a) slope area and (b) reference area for winters 2002-2016. Figure S5: IST difference between slope area and reference area and wind speed difference for winters 2002-2016. Figure S6: CCLM IST difference between surge (a)/slope area (b) and reference area and wind speed difference for April and May 2014. Figure S7: CCLM IST difference between (a) surge and (b) slope area and reference area and wind speed difference for winters 2002–2016. Figure S8: CCLM IST as a function of wind speed as for the daily means for 2 May 2014 (a) for the ice shelf areas of BIS and RLIS and (b) for the slope area. Table S1: Statistics for the linear regressions.

Author Contributions: Conceptualization, G.H.; Methodology, G.H., L.G., S.W.; Software, L. Glaw, S.W.; Formal Analysis, L.G.; Data Curation, L.G., S.W.; Writing-Original Draft Preparation, G.H.; Writing-Review & Editing, G.H., L.G., S.W.; Visualization, G.H., L.G.; Supervision, G.H.; Project Administration, G.H.; Funding Acquisition, G.H., S.W.

Funding: This research was partly funded by the Deutsche Forschungsgemeinschaft under grant numbers HE 2740/19, HE 2740/22 and WI 3314/3 in the framework of the priority programme SPP1158 "Antarctic Research with comparative investigations in Arctic ice areas". The publication was funded by the Open Access Fund of the University of Trier and the German Research Foundation (DFG) within the Open Access Publishing funding programme.

Acknowledgments: We thank Rolf Zentek for making the CCLM data available. MODIS data were obtained from NSIDC. The Quantarctica project (quantarctica.npolar.no) is also acknowledged.

Conflicts of Interest: The authors declare no conflict of interest. The funders had no role in the design of the study; in the collection, analyses, or interpretation of data; in the writing of the manuscript, and in the decision to publish the results.

References

1. Heinemann, G. Idealized simulations of the Antarctic katabatic wind system with a three-dimensional mesoscale model. *J. Geophys. Res.* **1997**, *102*, 13825–13834. [CrossRef]

2. van Lipzig, N.P.M.; Turner, J.; Colwell, S.R.; van den Broeke, M.R. The near-surface wind field over the Antarctic continent. *Int. J. Climatol.* **2004**, *24*, 1973–1982. [CrossRef]
3. Parish, T.R.; Bromwich, D.H. Reexamination of the Near-Surface Airflow over the Antarctic Continent and Implications on Atmospheric Circulations at High Southern Latitudes. *Mon. Weather Rev.* **2007**, *135*, 1961–1973. [CrossRef]
4. Phillpot, H.R.; Zillman, J.W. The surface temperature inversion over the Antarctic Continent. *J. Geophys. Res.* **1970**, *75*, 4161–4169. [CrossRef]
5. Loewe, F. The land of storms. *Weather* **1972**, *27*, 110–121. [CrossRef]
6. Ball, F.K. The Katabatic Winds of Adélie Land and King George V Land. *Tellus* **1957**, *9*, 201–208. [CrossRef]
7. Heinemann, G. Aircraft-Based Measurements Of Turbulence Structures In The Katabatic Flow Over Greenland. *Bound. Layer Meteorol.* **2002**, *103*, 49–81. [CrossRef]
8. Hudson, S.R.; Brandt, R.E. A Look at the Surface-Based Temperature Inversion on the Antarctic Plateau. *J. Clim.* **2005**, *18*, 1673–1696. [CrossRef]
9. Liu, H.; Jezek, K.; Li, B.; Zhao, Z. *Radarsat Antarctic Mapping Project Digital Elevation Model*; Version 2; National Snow and Ice Data Center: Boulder, CO, USA, 2001.
10. Bromwich, D.H. Satellite Analyses of Antarctic Katabatic Wind Behavior. *Bull. Am. Meteorol. Soc.* **1989**, *70*, 738–749. [CrossRef]
11. Rasmussen, L. *Greenland Winds and Satellite Imagery*; Vejret, Danish Meteorological Society: Copenhagen, Denmark, 1989; pp. 32–37.
12. Bromwich, D.H.; Carrasco, J.F.; Liu, Z.; Tzeng, R.-Y. Hemispheric atmospheric variations and oceanographic impacts associated with katabatic surges across the Ross ice shelf, Antarctica. *J. Geophys. Res.* **1993**, *98*, 13045–13062. [CrossRef]
13. King, J.C. Using satellite thermal infrared imagery to study boundary layer structure in an Antarctic katabatic wind region. *Int. J. Remote Sens.* **1998**, *19*, 3335–3348. [CrossRef]
14. Heinemann, G. On the Streakiness of Katabatic Wind Signatures on High-Resolution AVHRR Satellite Images: Results from the Aircraft-Based Experiment KABEG. *Polarforschung* **2000**, *66*, 19–30.
15. Ebner, L.; Heinemann, G.; Haid, V.; Timmermann, R. Katabatic winds and polynya dynamics at Coats Land, Antarctica. *Antarct. Sci.* **2014**, *26*, 309–326. [CrossRef]
16. Bromwich, D.H.; Carrasco, J.F.; Stearns, C.R. Satellite Observations of Katabatic-Wind Propagation for Great Distances across the Ross Ice Shelf. *Mon. Weather. Rev.* **1992**, *120*, 1940–1949. [CrossRef]
17. Klein, T.; Heinemann, G. On the forcing mechanisms of mesocyclones in the eastern Weddell Sea region, Antarctica: Process studies using a mesoscale numerical model. *Meteorol. Z.* **2001**, *10*, 113–122. [CrossRef]
18. Heinemann, G. Three-dimensional structures of summertime Antarctic meso-scale cyclones: Part I: Observational studies with aircraft, satellite and conventional data. *Glob. Atmos. Ocean Syst.* **1996**, *4*, 149–180.
19. Helm, V.; Humbert, A.; Miller, H. Elevation and elevation change of Greenland and Antarctica derived from CryoSat-2. *Cryosphere* **2014**, *8*, 1539–1559. [CrossRef]
20. Miliaresis, G.C. Spatiotemporal patterns of land surface temperature of Antarctica from MODIS monthly LST (MYD11C3) data. *J. Spat. Sci.* **2014**, *59*, 157–166. [CrossRef]
21. Liu, T.; Wang, Z.; Huang, X.; Cao, L.; Niu, M.; Tian, Z. An Effective Antarctic Ice Surface Temperature Retrieval Method for MODIS. *Photogramm. Eng. Remote Sens.* **2015**, *81*, 861–872. [CrossRef]
22. Meyer, H.; Katurji, M.; Appelhans, T.; Müller, M.; Nauss, T.; Roudier, P.; Zawar-Reza, P. Mapping Daily Air Temperature for Antarctica Based on MODIS LST. *Remote Sens.* **2016**, *8*, 732. [CrossRef]
23. Fréville, H.; Brun, E.; Picard, G.; Tatarinova, N.; Arnaud, L.; Lanconelli, C.; Reijmer, C.; van den Broeke, M. Using MODIS land surface temperatures and the Crocus snow model to understand the warm bias of ERA-Interim reanalyses at the surface in Antarctica. *Cryosphere* **2014**, *8*, 1361–1373. [CrossRef]
24. Wan, Z. Collection-6 MODIS Land Surface Temperature Products Users' Guide. Available online: https://lpdaac.usgs.gov/documents/118/MOD11_User_Guide_V6.pdf (accessed on 24 June 2019).
25. Riggs, G.A.; Hall, D.K. MODIS Sea Ice Products: User Guide to Collection 6. 17 March 2015.
26. Turner, J.; Bromwich, D.; Colwell, S.; Dixon, S.; Gibson, T.; Hart, T.; Heinemann, G.; Hutchinson, H.; Jacka, K.; Leonard, S.; et al. The Antarctic First Regional Observing Study of the Troposphere (FROST) Project. *Bull. Am. Meteorol. Soc.* **1996**, *77*, 2007–2032. [CrossRef]

27. Rockel, B.; Will, A.; Hense, A. The Regional Climate Model COSMO-CLM (CCLM). *Meteorol. Z.* **2008**, *17*, 347–348. [CrossRef]
28. Dee, D.P.; Uppala, S.M.; Simmons, A.J.; Berrisford, P.; Poli, P.; Kobayashi, S.; Andrae, U.; Balmaseda, M.A.; Balsamo, G.; Bauer, P.; et al. The ERA-Interim reanalysis: Configuration and performance of the data assimilation system. *Q. J. R. Meteorol. Soc.* **2011**, *137*, 553–597. [CrossRef]
29. Spreen, G.; Kaleschke, L.; Heygster, G. Sea ice remote sensing using AMSR-E 89-GHz channels. *J. Geophys. Res.* **2008**, *113*, 14485. [CrossRef]
30. Schröder, D.; Heinemann, G.; Willmes, S. The impact of a thermodynamic sea-ice module in the COSMO numerical weather prediction model on simulations for the Laptev Sea, Siberian Arctic. *Polar Res.* **2011**, *30*, 6334. [CrossRef]
31. Kohnemann, S.H.E.; Heinemann, G.; Bromwich, D.H.; Gutjahr, O. Extreme Warming in the Kara Sea and Barents Sea during the Winter Period 2000–2016. *J. Clim.* **2017**, *30*, 8913–8927. [CrossRef]
32. Gutjahr, O.; Heinemann, G.; Preußer, A.; Willmes, S.; Drüe, C. Quantification of ice production in Laptev Sea polynyas and its sensitivity to thin-ice parameterizations in a regional climate model. *Cryosphere* **2016**, *10*, 2999–3019. [CrossRef]
33. Hall, D.K.; Key, J.R.; Case, K.A.; Riggs, G.A.; Cavalieri, D.J. Sea ice surface temperature product from MODIS. *IEEE Trans. Geosci. Remote Sens.* **2004**, *42*, 1076–1087. [CrossRef]
34. Key, J.R.; Collins, J.B.; Fowler, C.; Stone, R.S. High-latitude surface temperature estimates from thermal satellite data. *Remote Sens. Environ.* **1997**, *61*, 302–309. [CrossRef]
35. Heinemann, G.; Rose, L. Surface energy balance, parameterizations of boundary-layer heights and the application of resistance laws near an Antarctic Ice Shelf front. *Bound. Layer Meteorol.* **1990**, *51*, 123–158. [CrossRef]
36. Heinemann, G. The KABEG'97 field experiment: An aircraft-based study of katabatic wind dynamics over the Greenland ice sheet. *Bound. Layer Meteorol.* **1999**, *93*, 75–116. [CrossRef]
37. Boylan, P.; Wang, J.; Cohn, S.A.; Hultberg, T.; August, T. Identification and intercomparison of surface-based inversions over Antarctica from IASI, ERA-Interim, and Concordiasi dropsonde data. *J. Geophys. Res.* **2016**, *121*, 9089–9104. [CrossRef]
38. Zhang, Y.; Seidel, D.J.; Golaz, J.-C.; Deser, C.; Tomas, R.A. Climatological Characteristics of Arctic and Antarctic Surface-Based Inversions. *J. Clim.* **2011**, *24*, 5167–5186. [CrossRef]
39. Lenaerts, J.T.M.; Lhermitte, S.; Drews, R.; Ligtenberg, S.R.M.; Berger, S.; Helm, V.; Smeets, C.J.P.P.; Broeke, M.R.V.D.; van de Berg, W.J.; van Meijgaard, E.; et al. Meltwater produced by wind–albedo interaction stored in an East Antarctic ice shelf. *Nat. Clim. Chang.* **2017**, *7*, 58–62. [CrossRef]